Cooperativity of IGF2BP1 and ETV6-RUNX1 in the pathogenesis of ETV6- RUNX1 positive B-Cell Acute Lymphoblastic Leukemia

Gunjan Sharma
All India Institute of Medical Sciences
Tiffany M Tran
University of California, Los Angeles
Jaspal Bassi
University of California, Los Angeles
Yuande Tan
Cedars-Sinai Medical Center
Amit Kumar Jaiswal
University of California, Los Angeles
Christine Tso
University of California, Los Angeles
Ayushi Jain
All India Institute of Medical Sciences
Jay Singh
DR. B.R.A. Institute Rotary Cancer Hospital
Anita Chopra
DR. B.R.A. Institute Rotary Cancer Hospital
Archna Singh
All India Institute of Medical Sciences
Sameer Bakhshi
DR. B.R.A. Institute Rotary Cancer Hospital
Parthaprasad Chattopadhyay
All India Institute of Medical Sciences
David Casero
Cedars-Sinai Medical Center
Dinesh Subba Rao
University of California, Los Angeles
Jayanth Kumar Palanichamy (drjayanth@aiims.edu)
All India Institute of Medical Sciences

Research Article

Keywords: IGF2BP1, ETV6-RUNX1 positive B-ALL, NFκB/TNFα signalling, Integrated RNA/RIP-Seq

Posted Date: May 31st, 2022

DOI: https://doi.org/10.21203/rs.3.rs-1691465/v1

Abstract

Background

ETV6-RUNX1 is the most prevalent translocation in pediatric B-ALL (B-cell Acute Lymphoblastic Leukemia). However, the exact pathogenesis of this translocation leading to leukemogenesis remains unclear. Insulin like Growth Factor 2 Binding Protein 1 (IGF2BP1), an oncofetal RNA binding protein (RBP), is overexpressed in *ETV6-RUNX1* positive B-ALL. We intended to investigate the role of IGF2BP1 in leukemogenesis in this study.

Methods

qRT-PCR was used to analyze *IGF2BP1* overexpression in an Indian cohort of pediatric B-ALL (*n = 167*). *IGF2BP1* and *ETV6-RUNX1* were knocked out in Reh, an *ETV6-RUNX1* positive B-ALL cell line, using CRISPR/Cas9 technology. Cell proliferation assays were used to study cell survival after *IGF2BP1*/*ETV6-RUNX1* KO and prednisolone response. RNA-Sequencing after IGF2BP1 knockout and RNA Immunoprecipitation sequencing (RIP-Seq) after IGF2BP1 pulldown were performed to find the putative targets of IGF2BP1. Luciferase reporter assays were used to study downstream mRNA target stability as well as pathways regulated by IGF2BP1. Finally, to study the *in-vivo* synergistic effect between ETV6-RUNX1 fusion protein and IGF2BP1, a murine bone marrow transplant model was utilized followed by flowcytometric analysis of hematopoietic tissues and histopathological examination.

Results

IGF2BP1 expression was found to be essential for tumor cell survival in Reh cell line. Knockout of *IGF2BP1* or *ETV6-RUNX1* led to reduced proliferation and increased sensitivity to prednisolone hinting at synergism between both the genes. Integrated analysis of transcriptome sequencing after IGF2BP1 knockout and RIP-Seq revealed that IGF2BP1 targets encompass multiple pro-oncogenic signalling pathways including TNFα/NFκB and PI3K-Akt pathways. Dysregulation of these pathways was also observed in patient samples. Mechanistically, we demonstrate that IGF2BP1 binds and stabilizes *ETV6-RUNX1* fusion transcript and the presence of a positive feedback loop between them which maintains a constitutive dysregulation of several oncogenic pathways.

Background

Acute lymphoblastic leukemia (ALL) is the most common pediatric malignancy with ~ 85% being of B-cell origin (B-ALL) [1]. B-ALL is characterized by the presence of different translocations including *BCR-ABL, ETV6-RUNX1, E2A-PBX1, MLL* fusion rearrangement, and several novel subtypes classified by gene expression signatures [2]. *ETV6-RUNX1* is the most common translocation with an incidence of ~ 25% in Western countries and a lower incidence in India and its neighboring countries [3, 4]. The *ETV6-RUNX1*

fusion occurs as an early, prenatal event in-utero and results in the formation of a pre-leukemic clone [5] which converts to ALL at a later stage after acquiring secondary mutations [6]. Despite its association with a good prognosis, some ETV6-RUNX1 patients have an overall poorer prognosis, usually associated with relapse [7].

ETV6-RUNX1 is a weak oncogene and its enforced expression in mouse hematopoietic stem cells (HSCs)/committed progenitors does not result in the development of B-ALL. Leukemia development was observed at a low penetrance when combined with loss of one of the alleles of *Kdm5c*/ *Pax5*/ *Cdkn2a* or when exposed to infections [8–10].

IGF2BP1, an oncofetal RNA binding protein (RBP), is known to be overexpressed in several cancers [11] including B-ALL [12]. IGF2BP1 has been seen to promote leukemic stem cell (LSC) maintenance and survival [13]. A GWAS study identified IGF2BP1 expression to be unique in *ETV6-RUNX1* translocation positive B-ALL patients [14]. *ETV6-RUNX1* transcript is a known target of IGF2BP1 [12]. Overexpression of *IGF2BP1* in the bone marrow has been found to be highly specific for diagnosing the presence of the *ETV6-RUNX1* translocation [15].

In this study, we extend our current knowledge in understanding the role of IGF2BP1 overexpression in expediting the pathogenesis of *ETV6-RUNX1* positive B-ALL. We demonstrate *IGF2BP1* overexpression in *ETV6-RUNX1* B-ALL patient samples and also show the presence of prednisolone resistance and relapses in a subset of these patients. CRISPR mediated knockout of *IGF2BP1* or *ETV6-RUNX1* led to reduced tumor cell survival and reversal of prednisolone resistance. The transcriptome regulated by IGF2BP1 included numerous pro-oncogenic signalling pathways including the TNF alpha/NFκB and the PI3K-Akt pathways. We validated the upregulation of some of these putative IGF2BP1 target genes in a B-ALL patient cohort.

A bone marrow transplant model co-expressing ETV6-RUNX1 and IGF2BP1 in lethally irradiated mice led to the development of a pre-leukemic phenotype that included clonal expansion in the bone marrow which was primarily led by uncommitted, progenitor proliferation. Overall, our results suggest that IGF2BP1 plays an important role in the pathogenesis of *ETV6-RUNX1* leukemia through multiple oncogenic pathways and can be utilized as an ideal therapeutic target for this particular subtype.

Methods

Patient sample collection and processing

Treatment naïve B-ALL patient bone marrow (BM) samples were collected from March 2016 to December 2020 at BR Ambedkar Institute Rotary Cancer Hospital at AIIMS, New Delhi. The study was approved by the Institutional Ethics and Biosafety Committees (IEC-1950/1.04.2016, RP-20/2016). Samples were collected after informed consent from a guardian and assent was taken from children > 7 years of age in accordance with the Declaration of Helsinki regulations. In addition, some archival BM samples,

preserved from previous studies, were also utilized after proper ethics clearance. Peripheral blood from healthy controls was also collected.

Cell Culture

The human cell lines HEK 293T (*ATCC*® *CRL3216*™), Reh (*ATCC* CRL-8286), murine pre-B-ALL cell line 7OZ/3 (*ATCC*® TIB-158™) were obtained from American Type Culture Collection (ATCC) and maintained as described previously [16].

Rna Isolation And Real-time Pcr

Total RNA was extracted from BM/cell lines using the TRIzol (Takara) method. 500-1000ng of RNA was reverse transcribed to cDNA using MMLV RT (Thermo Scientific, USA). Real Time PCR was performed to quantify gene expression using TB Green Premix Ex II (Takara). *RNA Polymerase II* and *PPIA* were used as internal controls for mammalian cell lines and m*Gapdh* and m*L32* for murine cell lines. ΔΔCt method was used to compare the gene expression [17].

Crispr/cas9 Ko

Reh-Cas9 was created by transducing Reh with LentiCas9-GFP overexpressing lentiviruses. Guide RNAs were designed using the Zhang lab website (http://crispr.mit.edu/) and cloned into pLKO5-EFS-tRFP vector [18]. Lentiviruses and retroviruses were generated as previously described [19].

Statistical Analysis

The patients were followed up in the Medical Oncology department, BRAIRCH, AIIMS. The last follow up was upto December 31, 2021. Overall survival (OS) was calculated as the time duration from date of diagnosis to death or last follow-up. Event free survival (EFS) was calculated as the time duration from date of diagnosis to the date of last follow-up or the first event (relapse or death). The probability of EFS and OS was calculated by the Kaplan-Meier method, with the differences compared using a two-sided log-rank test. All *in-vitro* experiments were repeated at least thrice. Mouse experiments were done at least twice. Comparison between different groups was done using Mann Whitney (two groups) /Kruskal-Wallis (more than two groups) statistical tests wherever applicable using GraphPad Prism software version 5 or SPSS statistical software package v20. A p-value of < 0.05 was considered to be significant. Additional methods and reagent details are provided in the Supplementary Methods and Tables 1–5.

Results

IGF2BP1 expression is specific to ETV6-RUNX1 positive patient samples

We had earlier reported the overexpression of *IGF2BP1* by RT-qPCR in the bone marrow of patients belonging to the *ETV6-RUNX1* subtype in a cohort of Indian patients (n=114) [20]. Additional samples

were added to the same cohort (Total n=167). *IGF2BP1* expression was found to be significantly higher (>1000 fold) in *ETV6-RUNX1* subtype, (median value = 2.34) compared to *ETV6-RUNX1* negative samples (median value = 0.0022) (p <0.0001) (*Fig. 1A*).

The presence of the *ETV6-RUNX1* translocation also correlated with lower White Blood Corpuscle (WBC) counts (*Fig. 1B*). For analyzing prednisolone response, the samples were stratified into *ETV6-RUNX1* positive and negative groups. The negative group included patients from the other translocations group (*BCR-ABL1*, *E2A-PBX1* and *MLL*) and the No Known Sentinel Translocation (NKST) group. We observed a higher proportion of Prednisolone Poor Responders (PPRs) among the *ETV6-RUNX1* positive patients (38% vs 26%) which was statistically non-significant (*Fig. 1C*).

The presence of this translocation correlated with a better overall survival as well as lower percentage of deaths (p=0.034, NKST vs E6R1+ and p<0.0001, E6R1- vs E6R1+) (median survival 39 months for NKST and 21 months for E6R1- patients and >60 months for E6R1+ patients) (*Fig. 1D*) which corroborates with existing literature [21]. Despite showing a better event free survival (p=0.017, NKST vs E6R1+ and p<0.0001, E6R1- vs E6R1+) (median survival was 56 months for E6R1+ patients compared to 33 months for NKST and 19 months for E6R1- patients), around 23% of the *ETV6-RUNX1* positive patients relapsed (*Fig. 1E*).

IGF2BP1 loss of function inhibits B-ALL cell proliferation and reverses prednisolone resistance

IGF2BP1 expression was observed to be significantly higher in Reh (*ETV6-RUNX1* translocated) cell line when compared to other leukemic cell lines (*Fig. 2A*). To examine the effects of the loss of IGF2BP1, knockout was performed in Reh-Cas9 cell line using 3 different sgRNAs (sg1-3) which were designed and cloned as described previously [18] (*Fig. 2B*). Knockout was confirmed by Western Blotting with sg1 and sg2 causing complete knockout (*Fig. 2C*). *IGF2BP1* knockout led to a significant decrease in cell proliferation as seen by the MTS assay.

IGF2BP1 knockout reversed prednisolone resistance and cells showed sensitivity to prednisolone with IC50 ~1 μM for both the guides used (*Fig. 2D-E*). Cells with the non-targeting gRNA (NT) were viable even at a 10 μM concentration of prednisolone, confirming resistance [22].

Integrated transcriptome and immunoprecipitation sequencing reveals overlap between IGF2BP1 and ETV6-RUNX1 regulated oncogenic pathways

To begin to unravel the mechanistic basis of our observations, the gene expression profile of *IGF2BP1* KO Reh cells was analysed by RNA-Seq. 88 transcripts showed upregulation and 270 transcripts showed downregulation (at least 2-fold change, p<0.05) after IGF2BP1 knockout. Gene Set Enrichment Analysis (GSEA) [23] revealed a significant negative enrichment of the TNFα signalling via NFκB, hypoxia and cholesterol metabolism pathways (*Fig. 2E*) in KO cells as compared to non-targeting controls. A significant positive enrichment was found for pathways regulating cell cycle and proliferation including G2M checkpoint and the MYC targets (*Fig. 2F*).

To gain insights into the mRNA interactome of IGF2BP1, we performed RNA Immunoprecipitation followed by high throughput sequencing (RIP-Seq) (*Fig. 3A*). Application of SETEN [24], a GSEA-based tool for RNA-binding proteins, revealed enrichment of putative IGF2BP1 targets in numerous pro-oncogenic signaling pathways. The ENRICHR tool [25] classified IGF2BP1 target transcripts to be involved in B-cell and myeloid malignancies using the GWAS catalogue database. GO biological processes and molecular functions revealed enrichment for RNA processing, translation and RNA degradation pathways (*Fig. 3B*, *Supplementary Fig.S1A-D*).

An integrated analysis of the *IGF2BP1*-KO RNA-Seq and IGF2BP1 RIP-Seq in Reh cells was performed. Initially, we did not observe a significant enrichment between IGF2BP1 putative targets (RIP-Seq log2 fold>0, *Fig. 3C*) and the direction of regulation after *IGF2BP1* deletion. However, integrating both datasets using GSEA (*Fig. 3D*) showed that the genes most downregulated after IGF2BP1 deletion were preferentially classified as IGF2BP1 putative targets (highest RIP-Seq enrichment, familywise error-rate p-value<0.003, *Fig. 3D*). This suggests that IGF2BP1 promotes RNA stability in Reh cells. Interestingly, genes up-regulated after IGF2BP1 KO were preferentially not enriched in the RIP data (familywise error-rate p-value<0.001, *Fig. 3D*) suggesting that these genes are indirectly regulated by IGF2BP1 (*Fig.3C-D*).

Combined pathway analysis of IGF2BP1 KO/RIP gene sets revealed that some of the significantly dysregulated pathways after the knockout also had many genes enriched in the RIP-Seq suggesting direct binding and regulation (*Fig.3E, Supplementary Data*). Examples include the TNFα/NFκB signaling and Hypoxia pathways. Oxidative phosphorylation was upregulated after knockout while cholesterol metabolism was downregulated. However, both were not RIP targets implying an indirect or downstream effect of *IGF2BP1* knockout on those pathways. A deeper analysis of genes within these pathways showed that some of the genes in the metabolism of RNA, oxidative phosphorylation, MTORC1 and MAPK pathways showed enrichment in the RIP dataset (*Fig.3F*).

TNFα induced NFκB and PI3K-Akt signalling pathways are activated in ETV6-RUNX1 positive B-ALL by IGF2BP1

We then aimed to map IGF2BP1-induced gene expression changes to expression signatures of different patient subtypes. We applied GSEA to compare our *IGF2BP1*-KO data to differential gene expression between *ETV6-RUNX1*, *E2A-PBX1* and *MLL* positive patients (from GSE65647, n=44) [16]. We also analyzed a dataset which compared *ETV6-RUNX1* positive patients' gene expression (n=4) with normal CD19 positive B-cells (n=2) [26]. There was a significant overlap between genes overexpressed and pathways enriched in *ETV6-RUNX1* positive tumors and genes/pathways downregulated after deletion of *IGF2BP1* (*Fig.3G*, *Supplementary Fig.S2-S4*).

We used BTYNB, a functional inhibitor of IGF2BP1 [27] to validate its role in regulating the non-canonical TNFα/NFκB pathway. Treatment of Reh with BTYNB led to a dose dependent decrease in cell proliferation. BTYNB treatment led to a decrease in both *IGF2BP1* and *ETV6-RUNX1* fusion transcript expression by qPCR. BTYNB had no effect on the RL and Jurkat cell lines which express minimal levels of *IGF2BP1(Supplementary Fig. S5A-D).*

Reh cells were transduced with NFκB-Luc-dTomato plasmid [28] which consists of the NFκB consensus sequence upstream of the Luciferase reporter gene. These cells showed an increase in luminescence after treatment with TNFα. Pre-treatment of these cells with BTYNB led to a loss of this luminescence induction in a dose dependent manner (*Fig.4A-B*).

We further validated genes from the TNFα/NFκB and PI3K-Akt pathways in our patient samples along with MACS enriched CD19+ B-cells as controls (*Fig. 4C-D*). Many of these genes including *IL6ST*, *MDM2, CDK6* and *NGFR* showed significant upregulation in the *ETV6-RUNX1* positive patients.

ETV6-RUNX1 fusion transcript is stabilized by IGF2BP1

ETV6-RUNX1 fusion transcript has been shown to affect the functions of wild type *ETV6* as well as *RUNX1* in a dominant negative fashion [29]. We sub cloned the *ETV6-RUNX1* transcript from a pcDNA3.1-*ETV6-RUNX1* plasmid (a kind gift from Dr Anthony Ford, ICR, London) into a bicistronic, retroviral, murine overexpression vector *(Supplementary Fig. S6A)*. *ETV6-RUNX1* virus particles were produced as described previously [19] and used to overexpress the same in a murine pre-B-ALL cell line, 7OZ/3 in three serial dilutions. There was a dose dependent increase in *Igf2bp1* levels (*Fig. 5B*).

We performed *ETV6-RUNX1* KO using guides targeting the *ETV6-RUNX1* junction or the 5' ETV6 region as reported previously *(Supplementary Fig. S6B)* [30] in Reh cell line. We observed a decrease in cell proliferation and sensitivity to prednisolone similar to the phenotype seen with *IGF2BP1* KO (IC50=1.6/2/3.5 μM for sg1/2/3 respectively). This suggested the involvement of both the proteins in conferring a glucocorticoid-resistant phenotype to Reh cells. (*Fig. 5B-C*).

IGF2BP1-RIP followed by RT-PCR of immunoprecipitated RNA showed significant enrichment of the *ETV6-RUNX1* junction, 5'-UTR of *ETV6* and *ACTB (*positive control*)* in the RIP vs Input samples (*Fig. 5D*). In order to study the effect of IGF2BP1 on *ETV6-RUNX1* stability, we cloned the junction region downstream of firefly luciferase *(Supplementary Fig. S6C)*. Cotransfection of this vector with IGF2BP1 resulted in significantly increased luciferase activity (*Fig. 5E*). Complete knockout of *IGF2BP1 (sg1 and sg2)* significantly decreased *ETV6-RUNX1* transcript levels in Reh cells (*Fig. 5F*). This data demonstrated the regulation of IGF2BP1 by *ETV6-RUNX1* and its stabilization by the former.

IGF2BP1 and ETV6-RUNX1 synergize to cause clonal progenitor expansion in the murine bone marrow

To directly assess the synergism between ETV6-RUNX1 and IGF2BP1, we undertook an *in-vivo* experiment to examine the effects of enforced expression of both transgenes. Murine bone marrow transplant experiments were performed using retroviruses, synthesized and used as previously described [19] (*SupplementaryFig. S7A*). We cloned the human coding sequence of *IGF2BP1* into MIG (MSCV-IRES-GFP), a murine stem cell virus–based (MSCV) retroviral vector and used it along with the *ETV6-RUNX1* cloned in MICH (MSCV-IRES-mCherry). We confirmed the functionality of the vectors in expressing IGF2BP1 and ETV6-RUNX1 as well as the fluorescent markers (*Supplementary Fig. S7B–D and data not shown)*.

All groups had similar levels of engraftment as seen from the CD45.1 positivity (*data not shown)*. Clonal expansion was observed in the peripheral bleeds of mice expressing both ETV6-RUNX1 and IGF2BP1 (combination group) from weeks 4-16 with a constant increase. This was measured by the ratio of GFP+ mCherry+ cells to the total transfected cells (double positive ratio) (*Supplementary Fig. S8A-B*).

Complete blood counts (CBC) at week 16 showed a decrease in mature B-cell counts after ETV6-RUNX1 overexpression and in the combination. There was an increase in total WBC counts after IGF2BP1 overexpression. In the combination, the number of mature red blood cells, platelets and neutrophils were significantly lower with an increase in immature reticulocyte counts (*SupplementaryFig. S9A-H*).

To further characterize these hematopoietic changes, mice were euthanized after 16 weeks and hematopoietic organs collected for analysis. The bone marrow counts were significantly higher in the combination group with significant clonal expansion. Analysis of the progenitors revealed significant increase in the Lin- population, hematopoietic stem cells (HSCs), Lymphomyeloid Primed Progenitors (LMPP) and common lymphoid progenitors (CLPs) (percentages and absolute counts) in the combination group. The ETV6-RUNX1 group also showed a small but significant increase in progenitor output (*Fig. 6A-6G*). Hardy fraction analysis of the bone marrow in the combination showed an accumulation of the pre-B cell population implying a B-cell developmental block. (*Supplementary Fig.S10*).

Previous studies have identified the Lin- c-Kit+ or the LSK (Lin- c-Kit+Sca1+) populations as leukemia initiating cells in different mouse models [31]. The bone marrow of the combination group showed a significant increase in both populations (*Fig. 7A)* with strong Ki67 positivity of the Lin- progenitor population implying an increased proliferation rate (*Fig. 7B*). The myeloid progenitors (common myeloid progenitors (CMP), granulocyte-monocyte progenitor (GMP) and megakaryocyte-erythroid progenitor (MEP)) were also significantly increased in the combination (*Supplementary Fig.S11*).

The progenitor populations from the bone marrow were analyzed for fluorescent marker expression (double positive (DP): mCherry+ GFP+ and double negative (DN): mCherry-GFP-). In the combination group, there was an increase in the Lin- population in both the DN and DP fractions implying both a cell extrinsic and intrinsic mechanism for progenitor expansion. Interestingly, the HSCs and LMPPs were only increased in the DP fraction indicating a purely cell intrinsic mechanism (*Supplementary Fig.S12*).

Histopathological examination of the bone marrow of mice expressing both ETV6-RUNX1 and IGF2BP1 showed marked hypercellularity along with a loss of normal architecture characterized by compressed vascular spaces, reduced fat globules and megakaryocytes (*Fig. 7C*). Spleens were significantly enlarged with clonal expansion (*Supplementary Fig.S13A-C*). The spleen was populated by immature cells including HSCs implying extramedullary hematopoiesis (*Supplementary Fig.S13D*). Histopathological analysis revealed loss of architecture with red pulp expansion and smaller germinal centers in the combination group (*Supplementary Fig.S13E*).

RT-qPCR from the bone marrow of the mice showed a significant increase in endogenous *Igf2bp1* levels after ETV6-RUNX1 overexpression, validating our in-vitro finding. The levels of *ETV6-RUNX1* and *IGF2BP1* were highest in the combination group (*Fig. 7D*).

Discussion

The molecular mechanism of ETV6-RUNX1 mediated leukemogenesis is incompletely understood. *ETV6-RUNX1* is known to be a weak oncogene unable to induce leukemia in the absence of secondary genetic alterations [9, 32]. As detected from the bloodspots in newborns, this translocation shows a far higher prevalence, with very few going on to develop leukemia supporting the 'two-hit' model of its molecular pathogenesis [33]. *Cdkn2a* loss, alterations of *Epor, Ebf1, Jak1, Jak3, Il2rb, Stat5* and *Trp53* have all been shown to synergize with ETV6-RUNX1 to cause leukemia in mice [32, 34]. We had previously identified that the RBP IGF2BP1 was specifically overexpressed in the *ETV6-RUNX1* translocated B-ALL and validated the same in a larger cohort [20]. The importance of RBPs in the pathogenesis of various leukemias including the IGF2BP family is slowly being dissected [35]. Our findings add to this existing knowledge of dysregulated RBP expression in *ETV6-RUNX1* translocated B-ALL.

B-ALL treatment at our cancer center is done using the Indian Childhood Collaborative Leukemia Group (ICiCLe) Protocol [36]. One of the risk stratification parameters includes percentage of blasts on day 8 after treatment with high dose prednisolone which divides patients into good and poor responders (PGR/PPR) [37]. Glucocorticoid resistance has been linked to poor prognosis and decreased event free survival [38]. The presence of *ETV6-RUNX1* translocation appears to correlate with a trend of prednisolone resistance. Although, the presence of *ETV6-RUNX1* correlated with a good prognosis as previously reported [39], the event free survival was inferior in comparison to the overall survival. These findings highlight the varied nature of response to chemotherapy and poorer prognosis in at least a subset of the *ETV6-RUNX1* positive patients.

Previously, loss of function of IGF2BP1 in epithelial cell lines has been shown to decrease cell proliferation and cause apoptosis [13, 40]. We found that knockout of *IGF2BP1* led to reduced cell proliferation and reversal of prednisolone resistance in Reh, an *ETV6-RUNX1* positive cell line. A similar phenotype was also observed after *ETV6-RUNX1* knockout. Interestingly, some of the pathways upregulated after *IGF2BP1* knockout are known to be upregulated after *ETV6-RUNX1* knockdown [41]. Knockout of *IGF2BP1* also led to a decrease in the expression of *ETV6-RUNX1* transcript and overexpression of ETV6-RUNX1 lead to a dose dependent increase in *IGF2BP1* levels implying interdependency between the two genes. Previous studies have also identified *ETV6-RUNX1* to be a target of IGF2BP1 and a 17q21 polymorphism within IGF2BP1 to be having a strong association with ETV6-RUNX1 positive B-ALL [14, 42].

A mechanistic examination of the transcriptome controlled by IGF2BP1 was analysed via a combined interrogation of the RIP-Seq/*IGF2BP1* KO RNA-Seq datasets which revealed enrichment of numerous pro-oncogenic pathways. Many pathways regulated by IGF2BP1 were also significantly associated with

ETV6-RUNX1 positive tumors, implying some degree of cooperativity between the two genes in disease pathogenesis.

IGF2BP1 appeared to bind and stabilize genes in the TNFα mediated non-canonical NFκB pathway which was also validated in our patient cohort. The non-canonical NFκB pathway is known to play an important role in inflammation [43]. In ETV6-RUNX1 translocated tumors, it may be contributing to creating an inflammatory environment within the bone marrow niche for the maintenance or emergence of the leukemic clones as reported previously [44]. An in-vitro NFκB mediated luciferase reporter assay showed a decrease in luciferase activity after IGF2BP1 inhibition underscoring the clear role of IGF2BP1 in regulating this pathway.

Interestingly, the pathways which were negatively enriched in the *IGF2BP1* KO cells were all positively enriched in the ETV6-RUNX1 positive tumors and vice versa. A recent study has demonstrated that ETV6-RUNX1 functions by competing for RUNX1 binding sites and leads to transcriptional repression of RUNX1 targets. The study also showed *ETV6-RUNX1* knockdown leading to an increase in the G2M checkpoint, E2F and MYC target pathways. These pathways were also upregulated after *IGF2BP1* knockout further establishing a role for their synergism [45].

RIP-Seq identified numerous pro-oncogenic pathways including the PI3K-Akt and MAPK pathways. Interestingly, some targets identified in RIP-Seq were not significantly downregulated after *IGF2BP1* knockout implying a multifactorial regulation of their mRNA stability. A qPCR validation of PI3K-Akt pathway genes (*MDM2*, *CDK6*, *CCND1*, *NGFR*) demonstrated a significantly high expression in *ETV6-RUNX1* positive patients. ETV6-RUNX1 is known to increase MDM2 which normally degrades p53 [46]. Interestingly, MDM2 is also known to have a p53-independent role in childhood ALL where its elevated expression induces expression of p65 subunit of NFκB and augments chemoresistance [47]. We had previously demonstrated *CDK6* to be a target of IGF2BP3 in ALL suggesting some degree of overlap between targets of this family [16]. Cyclin D1 (CCND1) is required during the transition from G1 to S phase and is known to be overexpressed in B-cell lymphomas [48]. *CCND1* expression is associated with poor prognosis and relapse in childhood ALL [49]. High NGFR expression has been known to be associated with *ETV6-RUNX1* rearrangement [50].

To study the pathogenetic role of IGF2BP1 in leukemia development, we developed the first in-vivo model with enforced expression of IGF2BP1 in the hematopoietic system. The combination of IGF2BP1 and ETV6-RUNX1 led to a hypercellular bone marrow along with increased progenitor output across all lineages (HSCs, LMPPs, CLPs and myeloid progenitors). The peripheral blood showed a decrease in mature cells and increase in the immature cells over time. Together, these findings suggest that the combination of ETV6-RUNX1 and IGF2BP1 promotes skewing of BM development towards an immature phenotype. These progenitor cells were hyperproliferative as seen by Ki67 staining. There was significant clonal expansion of these double positive cells. ETV6-RUNX1 overexpression alone led to a small but significant increase in progenitor output as reported previously [8, 9, 34]. This progenitor expansion appeared to be fuelled by both cell extrinsic and intrinsic mechanisms indicating that the combination led

to an altered marrow niche favouring proliferation. IGF2BP1 has been shown to maintain stem cell properties by regulating *HOXB4*, *ALDH1A1* and *MYB* in leukemic cell lines [13]. Histopathological analysis confirmed the hypercellular and disrupted architecture in the marrow and spleen and concomitant extramedullary hematopoiesis. ETV6-RUNX1 overexpression managed to increase endogenous *Igf2bp1* levels in the bone marrow thus providing proof of our *in-vitro* finding.

Overexpression of ETV6-RUNX1 has been shown to increase HSCs with increased quiescence. Mature B-cell output has been known to be decreased with a developmental block at the pro-B cell stage [8]. In our combination experiments, Hardy fraction analysis showed an expansion of the small and large pre-B cell fractions indicating a developmental arrest. It is interesting to speculate a co-operative role for ETV6-RUNX1 and IGF2BP1 where the ETV6-RUNX1 promotes the progenitor expansion and prevents B-cell maturation which are then driven towards further expansion and leukemogenesis by the pro-oncogenic pathway genes stabilized by IGF2BP1.

Although the mice did not develop overt leukemia by 16 weeks, the observed features appear to mimic a pre-leukemic phenotype. Our findings appear to agree with previous studies which show that secondary hits are necessary for leukemogenesis even after ETV6-RUNX1 overexpression in mouse HSCs [9]. Due to its weak oncogenic nature, only a fraction of children with the ETV6-RUNX1 translocation go on to develop B-ALL. The positive feedback shown between ETV6-RUNX1 and IGF2BP1 may develop over time, leading to an incrementally altered transcriptome and the eventual emergence of a dominant transformed clone during leukemogenesis. By enforcing IGF2BP1 expression, we attempted to accelerate this process; and our data bears out this additive/synergistic relationship.

Our work uncovers a posttranscriptional, pro-oncogenic program driven by IGF2BP1 in ETV6-RUNX1 positive B-ALL. At the functional level, we have characterized and validated the differential activity of the non-canonical NFκB and PI3K-Akt pathways. These pathways are also reinforced by the feedback between ETV6-RUNX1 and IGF2BP1. With many of these pathways being druggable and a small molecule inhibitor for IGF2BP1 available, our work lays the foundation for novel combinatorial therapeutic approaches in *ETV6-RUNX1* positive leukemias.

Conclusion

A murine model of ETV6-RUNX1 and IGF2BP1 overexpression has not been created before. This is the first time that such a model has been created using sequential retroviral infection. We have observed a novel pre-leukemic phenotype which has not been reported in any of the previous studies. Thus, our *in-vivo* mouse model supports the critical role of IGF2BP1 overexpression as a secondary hit and also confirmed the *in-vitro* finding of synergism between these two proteins. The next interesting thing will be to use IGF2BP1 as a therapeutic target for this particular subtype of leukemia.

Abbreviations

B-ALL
B-Acute Lymphoblastic Leukemia
IGF2BP1
Insulin like growth factor 2 binding protein 1
EFS
Event free survival
OS
Overall survival
qRT-PCR
quantitative real-time polymerase chain reaction
HSC
Hematopoietic stem cell
PGR
Prednisolone good responder
PPR
Prednisolone poor responder
RIP
RNA immunoprecipitation
MACS
Magnetic activated cell sorting

Declarations

Ethics approval and consent to participate

The study was approved by the Institutional Ethics and Biosafety Committees (IEC-1950/1.04.2016, RP-20/2016). Samples were collected after informed consent from a guardian and assent was taken from children >7 years of age in accordance with the Declaration of Helsinki regulations. In addition, some archival BM samples, preserved from previous studies, were also utilized after proper ethics clearance.

All mouse experimental procedures were conducted with the approval of the UCLA Chancellor's Animal Research Committee (ARC).

Consent for publication

Not applicable.

Availability of Supporting Data:

All data generated or analyzed during this study are included in this published

article and its supplementary information files. The analyzed RNA-Seq and RIP-Seq data can be found in a data supplement. Raw reads are available in the SRA database with BioProject ID PRJNA837729.

Competing interests

All authors declare no potential conflict of interest.

Funding

This work was supported by the Wellcome Trust/DBT India Alliance Early Career Fellowship to JKP (IA/CPHE/15/1/502050). GS was supported by a DBT Senior Research Fellowship as well as a SERB Overseas Visiting Doctoral Research Fellowship. JS was supported by a DBT Senior Research Fellowship and AJ by a CSIR Senior Research Fellowship. DSR was supported by grants from the National Institutes of Health/ National Cancer Institute (R21CA197441, R01CA264986). TMT was supported by the Tumor Cell Biology Training Grant NIH T32 CA009056.

Authors' Contributions

Conceptualization: JKP

Experimental Methodology and Data analysis: JKP, GS, TMT, JB, AKJ, CT, PC

Patient sample collection and clinical data analysis: AJ, GS, JS, SB, AS and AC

Bioinformatic Analysis: YT and DC carried out bioinformatic analysis.

Histopathology and data analysis: DSR

Project administration: JKP

Writing – original draft: GS, JKP

Writing – review and editing: All authors reviewed and edited the manuscript. They also provided critical feedback and helped in shaping the research and manuscript.

Acknowledgments

We thank Prof Kenneth Dorshkind and all our collaborators for vibrant discussions regarding the experiments and data. We would like to thank Dr. Anthony Ford, ICR London for the kind gift (pcDNA3.1-*TEL-AML1* plasmid). The pHAGE6 vector was a kind gift from Dr Alejandro B. Balazs, Ragon Institute, MIT, MGH and Harvard. The pHAGE2-NFKB-TA-Luc-UBC-dTomato was a gift from Dr Darrell Kotton (Addgene plasmid # 49335) and pLKO5.sgRNA.EFS.tRFP was a gift from Dr Benjamin Ebert (Addgene plasmid # 57823).

Authors' information

[1]Department of Biochemistry, All India Institute of Medical Sciences, New Delhi, India

[2]Department of Pathology and Laboratory Medicine, David Geffen School of Medicine, University of California, Los Angeles, California, USA

[3]F. Widjaja Foundation Inflammatory Bowel and Immunobiology Research Institute, Cedars-Sinai Medical Center, Los Angeles, California, USA

[4]Department of Laboratory Oncology, Dr B.R Ambedkar Institute Rotary Cancer Hospital, All India Institute of Medical Sciences, New Delhi, India

[5] Department of Medical Oncology, Dr B.R Ambedkar Institute Rotary Cancer Hospital, All India Institute of Medical Sciences, New Delhi, India

References

1. Pui C-H, Robison LL, Look AT. Acute lymphoblastic leukaemia. Lancet (London, England). 2008;371(9617):1030–43.
2. Mullighan CG. How advanced are we in targeting novel subtypes of ALL? Best Pract Res Clin Haematol. 2019;32(4):101095.
3. Chopra A, Soni S, Verma D, Kumar D, Dwivedi R, Vishwanathan A, et al. Prevalence of common fusion transcripts in acute lymphoblastic leukemia: A report of 304 cases. Asia Pac J Clin Oncol. 2015;11(4):293–8.
4. Ganguly S, Kinsey S, Bakhshi S. Childhood cancer in India. Cancer Epidemiol. 2021;71(Pt B):101679.
5. Ford AM, Bennett CA, Price CM, Bruin MC, Van Wering ER, Greaves M. Fetal origins of the TEL-AML1 fusion gene in identical twins with leukemia. Proceedings of the National Academy of Sciences of the United States of America. 1998;95(8):4584–8.
6. Papaemmanuil E, Rapado I, Li Y, Potter NE, Wedge DC, Tubio J, et al. RAG-mediated recombination is the predominant driver of oncogenic rearrangement in ETV6-RUNX1 acute lymphoblastic leukemia. Nat Genet. 2014;46(2):116–25.
7. Bokemeyer A, Eckert C, Meyr F, Koerner G, von Stackelberg A, Ullmann R, et al. Copy number genome alterations are associated with treatment response and outcome in relapsed childhood ETV6/RUNX1-positive acute lymphoblastic leukemia. Haematologica. 2014;99(4):706–14.
8. Schindler JW, Van Buren D, Foudi A, Krejci O, Qin J, Orkin SH, et al. TEL-AML1 corrupts hematopoietic stem cells to persist in the bone marrow and initiate leukemia. Cell Stem Cell. 2009;5(1):43–53.
9. Rodríguez-Hernández G, Casado-García A, Isidro-Hernández M, Picard D, Raboso-Gallego J, Alemán-Arteaga S, et al. The Second Oncogenic Hit Determines the Cell Fate of ETV6-RUNX1 Positive Leukemia. Front Cell Dev Biol. 2021;9:704591.
10. Rodriguez-Hernandez G, Hauer J, Martin-Lorenzo A, Schafer D, Bartenhagen C, Garcia-Ramirez I, et al. Infection Exposure Promotes ETV6-RUNX1 Precursor B-cell Leukemia via Impaired H3K4 Demethylases. Cancer Res. 2017;77(16):4365–77.

11. Huang X, Zhang H, Guo X, Zhu Z, Cai H, Kong X. Insulin-like growth factor 2 mRNA-binding protein 1 (IGF2BP1) in cancer. J Hematol Oncol. 2018;11(1):88.
12. Stoskus M, Eidukaite A, Griskevicius L. Defining the significance of IGF2BP1 overexpression in t(12;21)(p13;q22)-positive leukemia REH cells. Leuk Res. 2016;47:16–21.
13. Elcheva IA, Wood T, Chiarolanzio K, Chim B, Wong M, Singh V, et al. RNA-binding protein IGF2BP1 maintains leukemia stem cell properties by regulating HOXB4, MYB, and ALDH1A1. Leukemia. 2020;34(5):1354–63.
14. Vijayakrishnan J, Qian M, Studd JB, Yang W, Kinnersley B, Law PJ, et al. Identification of four novel associations for B-cell acute lymphoblastic leukaemia risk. Nat Commun. 2019;10(1):5348.
15. Sharma G, Tran T, Bassi J, Jaiswal AK, Tso C, Jain A, et al. Synergism between IGF2BP1 and ETV6-RUNX1 in the Pathogenesis of ETV6-RUNX1 Positive B-Acute Lymphoblastic Leukaemia. Blood. 2021;138(Supplement 1):3483-.
16. Palanichamy JK, Tran TM, Howard JM, Contreras JR, Fernando TR, Sterne-Weiler T, et al. RNA-binding protein IGF2BP3 targeting of oncogenic transcripts promotes hematopoietic progenitor proliferation. J Clin Invest. 2016;126(4):1495–511.
17. Livak KJ, Schmittgen TD. Analysis of relative gene expression data using real-time quantitative PCR and the 2(-Delta Delta C(T)) Method. Methods (San Diego, Calif). 2001;25(4):402-8.
18. Shalem O, Sanjana NE, Hartenian E, Shi X, Scott DA, Mikkelson T, et al. Genome-scale CRISPR-Cas9 knockout screening in human cells. Science. 2014;343(6166):84–7.
19. O'Connell RM, Rao, D.S., Chaudhuri, A.A., Boldin, M.P., Taganov, K.D., Nicoll, J., Paquette, R.L., Baltimore, D.. Sustained expression of microRNA-155 in hematopoietic stem cells causes a myeloproliferative disorder. Journal of Experimental Medicine. 2008. 205;585–594.
20. Sharma G, Boby E, Nidhi T, Jain A, Singh J, Singh A, et al. Diagnostic Utility of IGF2BP1 and Its Targets as Potential Biomarkers in ETV6-RUNX1 Positive B-Cell Acute Lymphoblastic Leukemia. Frontiers in Oncology. 2021;11:114.
21. Inaba H, Mullighan CG. Pediatric acute lymphoblastic leukemia. Haematologica. 2020;105(11):2524–39.
22. Usami I, Imamura T, Takahashi Y, Suenobu SI, Hasegawa D, Hashii Y, et al. Discontinuation of L-asparaginase and poor response to prednisolone are associated with poor outcome of ETV6-RUNX1-positive pediatric B-cell precursor acute lymphoblastic leukemia. Int J Hematol. 2019;109(4):477–82.
23. Subramanian A, Tamayo P, Mootha VK, Mukherjee S, Ebert BL, Gillette MA, et al. Gene set enrichment analysis: A knowledge-based approach for interpreting genome-wide expression profiles. Proceedings of the National Academy of Sciences. 2005;102(43):15545–50.
24. Budak G, Srivastava R, Janga SC. Seten: a tool for systematic identification and comparison of processes, phenotypes, and diseases associated with RNA-binding proteins from condition-specific CLIP-seq profiles. RNA (New York, NY). 2017;23(6):836–46.
25. Kuleshov MV, Jones MR, Rouillard AD, Fernandez NF, Duan Q, Wang Z, et al. Enrichr: a comprehensive gene set enrichment analysis web server 2016 update. Nucleic acids research. 2016;44(W1):W90-W7.

26. Linka Y, Ginzel S, Kruger M, Novosel A, Gombert M, Kremmer E, et al. The impact of TEL-AML1 (ETV6-RUNX1) expression in precursor B cells and implications for leukaemia using three different genome-wide screening methods. Blood Cancer J. 2013;3:e151.
27. Mahapatra L, Andruska N, Mao C, Le J, Shapiro DJ. A Novel IMP1 Inhibitor, BTYNB, Targets c-Myc and Inhibits Melanoma and Ovarian Cancer Cell Proliferation. Transl Oncol. 2017;10(5):818–27.
28. Sethi G, Ahn KS, Pandey MK, Aggarwal BB. Celastrol, a novel triterpene, potentiates TNF-induced apoptosis and suppresses invasion of tumor cells by inhibiting NF-kappaB-regulated gene products and TAK1-mediated NF-kappaB activation. Blood. 2007;109(7):2727–35.
29. Gunji H, Waga K, Nakamura F, Maki K, Sasaki K, Nakamura Y, et al. TEL/AML1 shows dominant-negative effects over TEL as well as AML1. Biochem Biophys Res Commun. 2004;322(2):623–30.
30. Montaño A, Ordoñez, J.L., Alonso-Pérez, V., Hernández-Sánchez, J., Santos, S., González, T., Benito, R., García-Tuñón, I., Hernández-Rivas, J.M. ETV6/RUNX1 Fusion Gene Abrogation Decreases the Oncogenicity of Tumour Cells in a Preclinical Model of Acute Lymphoblastic Leukaemia. Cells. 2020. 9: 215.
31. Hu Y, Swerdlow S, Duffy TM, Weinmann R, Lee FY, Li S. Targeting multiple kinase pathways in leukemic progenitors and stem cells is essential for improved treatment of Ph < sup>+</sup > leukemia in mice. Proceedings of the National Academy of Sciences. 2006;103(45):16870-5.
32. Li M, Jones L, Gaillard C, Binnewies M, Ochoa R, Garcia E, et al. Initially disadvantaged, TEL-AML1 cells expand and initiate leukemia in response to irradiation and cooperating mutations. Leukemia. 2013;27(7):1570–3.
33. Kantner H-P, Warsch W, Delogu A, Bauer E, Esterbauer H, Casanova E, et al. ETV6/RUNX1 Induces Reactive Oxygen Species and Drives the Accumulation of DNA Damage in B Cells. Neoplasia. 2013;15(11):1292-IN28.
34. Tsuzuki S, Seto M, Greaves M, Enver T. Modeling first-hit functions of the t(12;21) TEL-AML1 translocation in mice. Proceedings of the National Academy of Sciences of the United States of America. 2004;101(22):8443–8.
35. Schuschel K, Helwig M, Hüttelmaier S, Heckl D, Klusmann J-H, Hoell JI. RNA-Binding Proteins in Acute Leukemias. International Journal of Molecular Sciences. 2020;21(10):3409.
36. Das N, Banavali S, Bakhshi S, Trehan A, Radhakrishnan V, Seth R, et al. Protocol for ICiCLe-ALL-14 (InPOG-ALL-15-01): a prospective, risk stratified, randomised, multicentre, open label, controlled therapeutic trial for newly diagnosed childhood acute lymphoblastic leukaemia in India. Trials. 2022;23(1):102.
37. Lee JW, Cho, B.. Prognostic factors and treatment of pediatric acute lymphoblastic leukemia. Korean Journal of Pediatrics. 2017;60:129.
38. Kaspers GJ VA, Pieters R, Van Zantwijk CH, Smets LA, Van Wering ER, Van Der Does-Van Den Berg A. In vitro cellular drug resistance and prognosis in newly diagnosed childhood acute lymphoblastic leukemia. Blood. 1997;90(7):2723–9.

39. Bhojwani D, Pei D, Sandlund JT, Jeha S, Ribeiro RC, Rubnitz JE, et al. ETV6-RUNX1-positive childhood acute lymphoblastic leukemia: improved outcome with contemporary therapy. Leukemia. 2012;26(2):265–70.
40. Bell JL, Wachter K, Muhleck B, Pazaitis N, Kohn M, Lederer M, et al. Insulin-like growth factor 2 mRNA-binding proteins (IGF2BPs): post-transcriptional drivers of cancer progression? Cell Mol Life Sci. 2013;70(15):2657–75.
41. Zaliova M, Madzo J, Cario G, Trka J. Revealing the role of TEL/AML1 for leukemic cell survival by RNAi-mediated silencing. Leukemia. 2011;25(2):313–20.
42. Stoskus M, Vaitkeviciene G, Eidukaite A, Griskevicius L. ETV6/RUNX1 transcript is a target of RNA-binding protein IGF2BP1 in t(12;21)(p13;q22)-positive acute lymphoblastic leukemia. Blood Cells Mol Dis. 2016;57:30–4.
43. Aggarwal BB. Nuclear factor-kappaB: the enemy within. Cancer Cell. 2004;6(3):203–8.
44. Beneforti L, Dander E, Bresolin S, Bueno C, Acunzo D, Bertagna M, et al. Pro-inflammatory cytokines favor the emergence of ETV6-RUNX1-positive pre-leukemic cells in a model of mesenchymal niche. Br J Haematol. 2020;190(2):262–73.
45. Wray JP, Deltcheva EM, Boiers C, Richardson SE, Chhetri JB, Gagrica S, et al. Cell cycle corruption in a pre-leukemic ETV6-RUNX1 model exposes RUNX1 addiction as a therapeutic target in acute lymphoblastic leukemia. bioRxiv. 2021:2020.12.22.423823.
46. Kaindl U, Morak M, Portsmouth C, Mecklenbrauker A, Kauer M, Zeginigg M, et al. Blocking ETV6/RUNX1-induced MDM2 overexpression by Nutlin-3 reactivates p53 signaling in childhood leukemia. Leukemia. 2014;28(3):600–8.
47. Gu L, Findley HW, Zhou M. MDM2 induces NF-κB/p65 expression transcriptionally through Sp1-binding sites: a novel, p53-independent role of MDM2 in doxorubicin resistance in acute lymphoblastic leukemia. Blood. 2002;99(9):3367–75.
48. Hydbring P, Malumbres M, Sicinski P. Non-canonical functions of cell cycle cyclins and cyclin-dependent kinases. Nat Rev Mol Cell Biol. 2016;17(5):280–92.
49. Elsayed GM, Ismail MM, Moneer MM. Expression of P-glycoprotein, Cyclin D1 and Ki-67 in Acute Lymphoblastic Leukemia: Relation with Induction Chemotherapy and Overall Survival. Indian J Hematol Blood Transfus. 2011;27(3):157–63.
50. Troeger A, Glouchkova L, Laws H-J, Hanenberg H, Meisel R, Janka-Schaub G, et al. High NGF Receptor Expression on ALL Blasts - A Novel Independent Prognostic Marker Identifying Patients with Favorable Outcome. Blood. 2005;106(11):1462-.

Figures

Figure 1

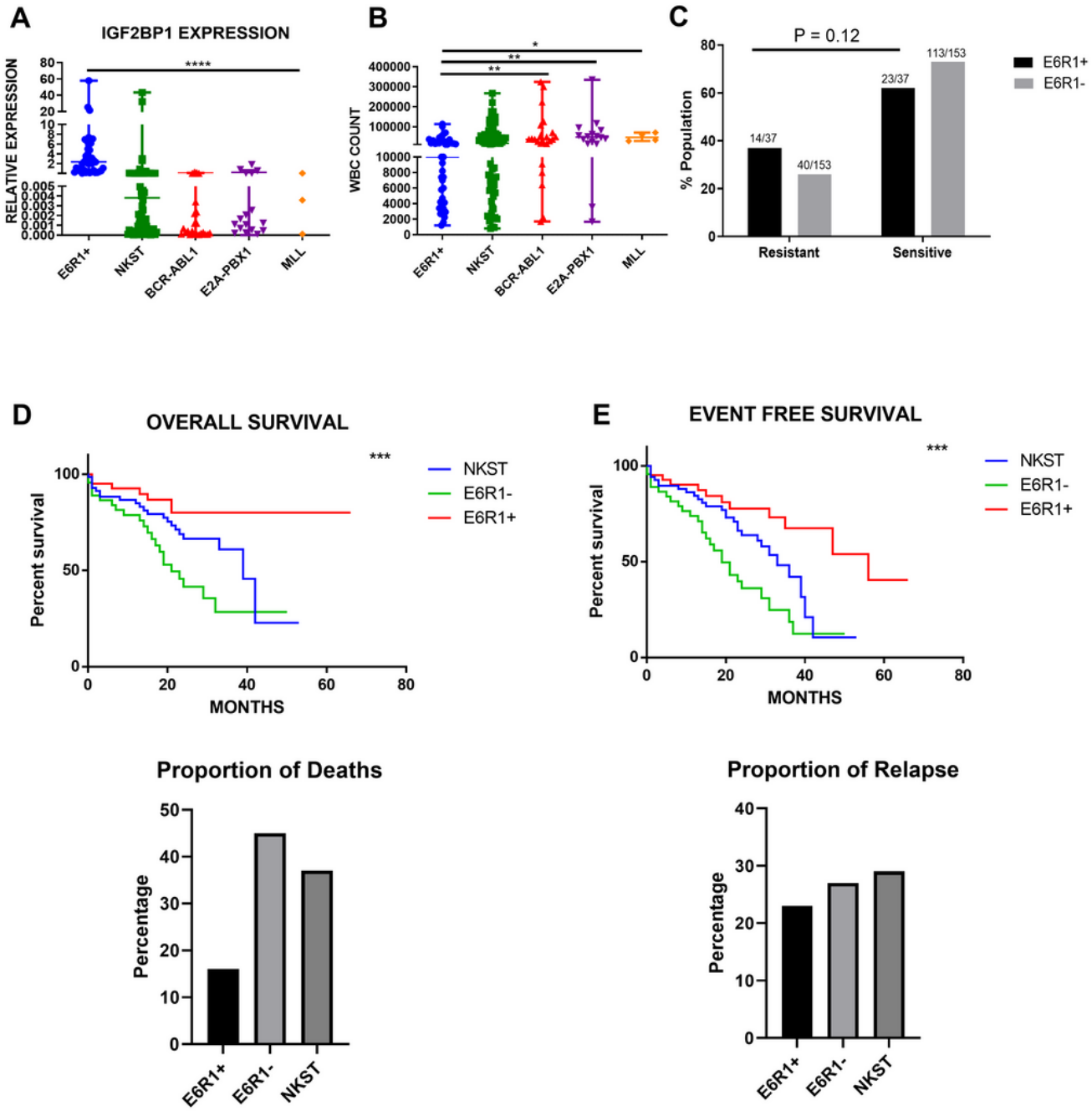

Figure 1

Expression of *IGF2BP1* and correlation with patient prognostic parameters. A) Real time expression data showing *IGF2BP1* overexpression in *ETV6-RUNX1* translocation positive patients (n=43), patients with no known sentinel translocation (n=76, includes patients with altered cytogenetics, n=13) and patients with other translocations (n=48, *BCR-ABL1* (n=27), *E2A-PBX1* (n=17), *MLL* (n=4)*)* B) WBC counts in B-ALL patient groups (****p<0.0001, ***p < 0.001, **p < 0.01, *p < 0.05) C) Percentage of prednisolone resistant

and sensitive patients in *ETV6-RUNX1* positive and negative subgroups (chi-square-test) D) Overall and E) Event free survival of B-ALL patients (N = 163) belonging to *ETV6-RUNX1* translocation positive group (E6R1+) (n = 43), other translocations group (E6R1-) (n = 44), No known sentinel translocation group (NKST) (n =76) (Kaplan-Meier method with Log-rank test; ***p < 0.001)

Figure 2

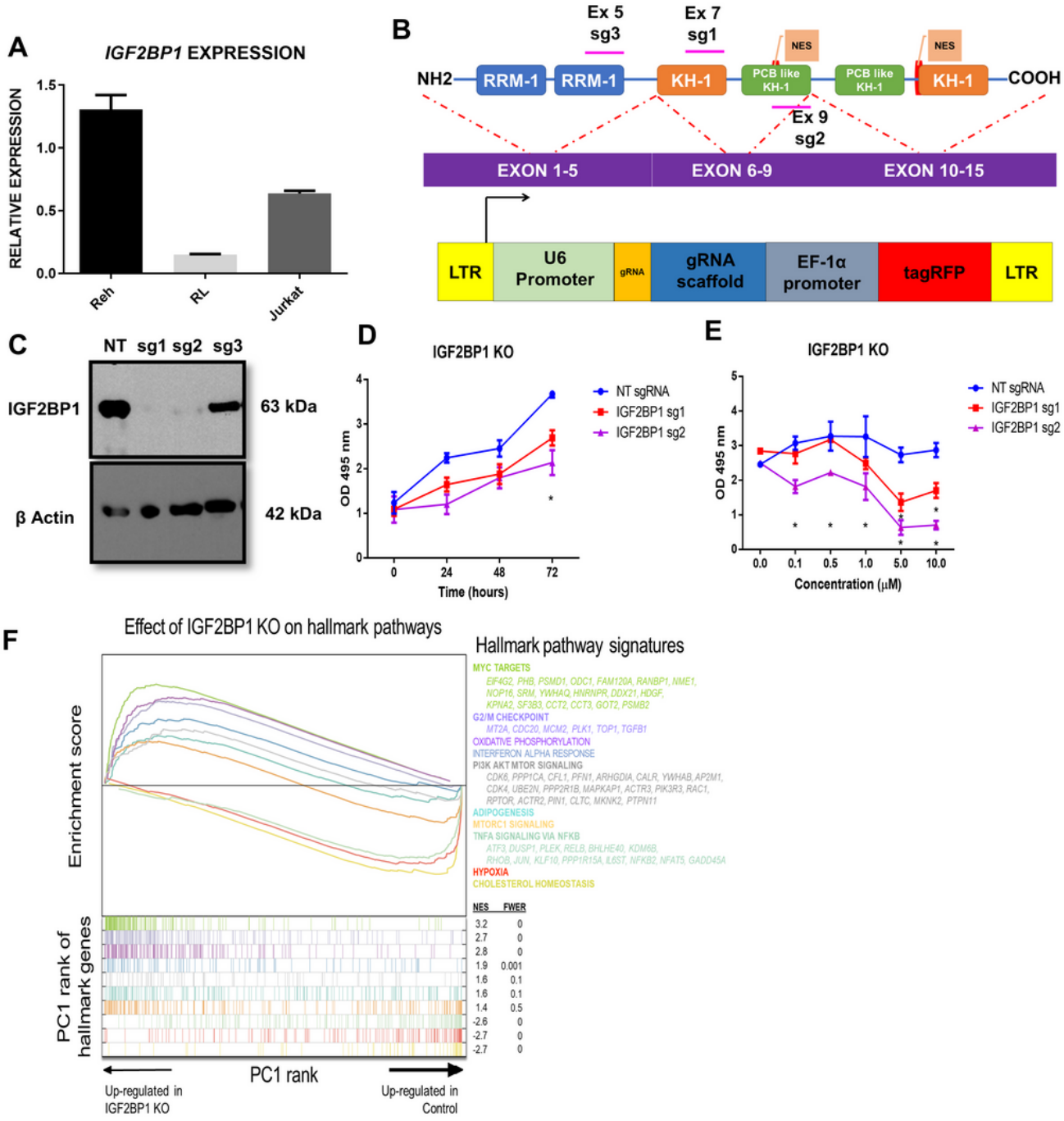

Figure 2

Effect of *IGF2BP1* knockout in *ETV6-RUNX1* positive cell line. A) mRNA expression of *IGF2BP1* in different ALL cell lines analyzed by qRT-PCR B) Schematic for cloning of guide RNAs targeted against different exons of *IGF2BP1* in pLKO5-tRFP vector C) Western blotting after knockout of IGF2BP1 in Reh Cas9-GFP cells with β-Actin as the loading control, NT (Non-targeting control) D) Cell proliferation of different IGF2BP1 KO clones as determined by MTS assay (t-test; *p < 0.05, **p < 0.01, ***p < 0.001, ****p < 0.0001) E) Effect of Prednisolone induced cytotoxicity in Reh-Cas9 cells after *IGF2BP1* KO using MTS assay F) Gene Set Enrichment Analysis (GSEA): Hallmark pathways enriched after RNA-Seq of IGF2BP1 KO in Reh-Cas9 cells; The x axis represents the pre-ranked list of genes based on PC1 loadings, which segregates between genes more expressed in IGF2BP1 KO cells (left) and wild type cells (right). Segment plots (bottom) highlight the position of genes from hallmark pathways in the pre-ranked list. The vertical axis in line plots (top) represents the cumulative Enrichment Score (ES) from GSEA, and NES is the overall normalized enrichment score (with FWER=familywise error rate) for each selected pathway. Color-coded names for some genes in selected pathways are shown

Figure 3

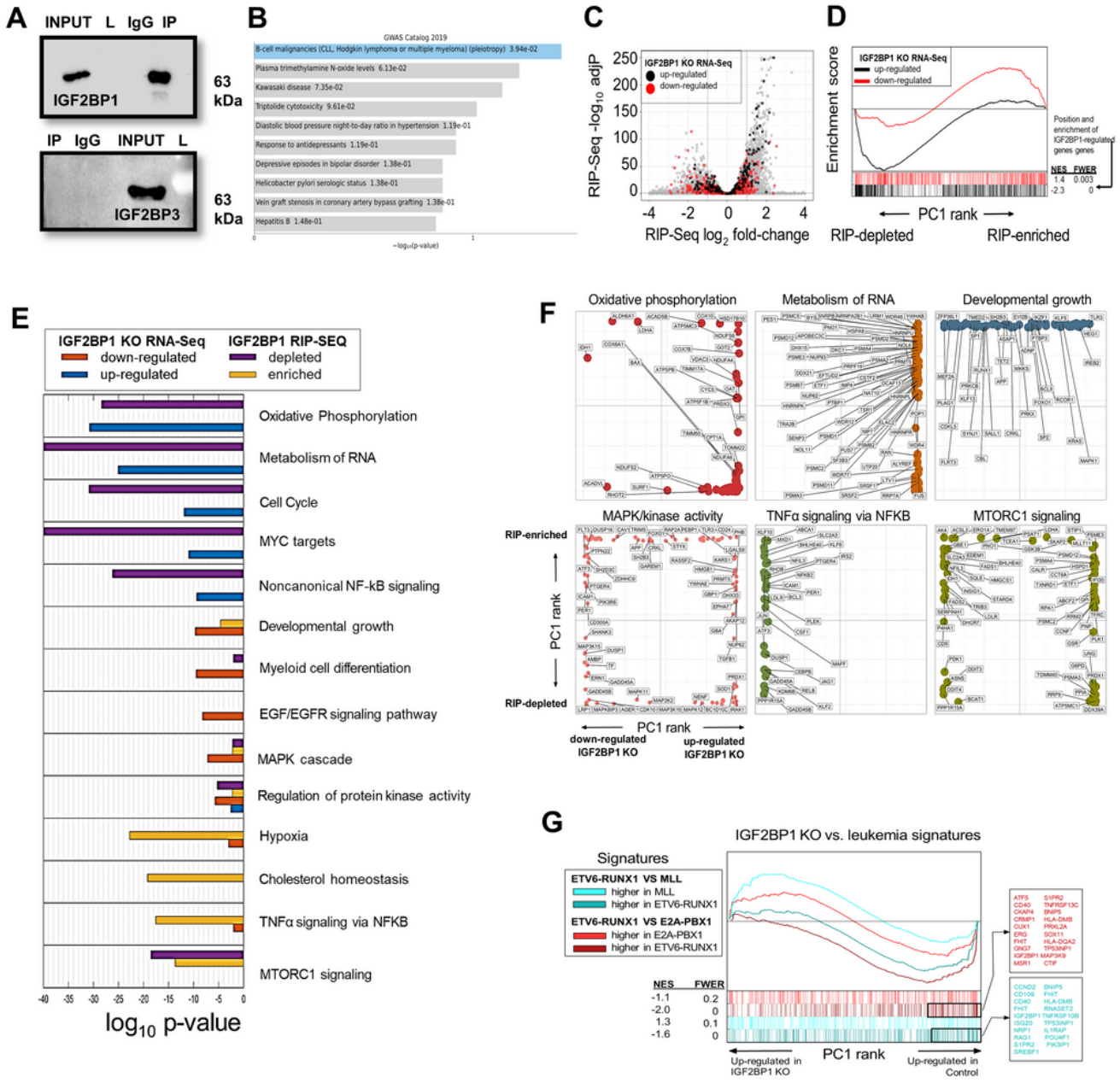

Figure 3

Identification of downstream pathways of IGF2BP1 in B-ALL. A) Western Blotting after RNA Immunoprecipitation of IGF2BP1 in Reh cell line; Specificity of the immunoprecipitation established by Western blotting analysis for another family member, IGF2BP3. B) Output of EnrichR package used to categorize the IGF2BP1 RIP targets using GWAS catalogue. C) Volcano plot of IGF2BP1 RIP-Seq data in Reh cell line. Genes up and down-regulated (RNA-Seq) after IGF2BP1 KO are highlighted as black and red

dots respectively D) GSEA analyzing the association between enrichment in IGF2BP1 RIP-Seq samples and genes regulated in IGF2BP1 KO cells. X axis represents the pre-ranked list of genes based on RIP-Seq PC1 loadings, which segregates between genes enriched (right) and depleted (left) in IP samples. Segment plots (bottom) highlight the position of genes strongly up/down regulated in IGF2BP1 KO cells. The vertical axis in line plots (top) represents the cumulative Enrichment Score (ES) from GSEA, and NES is the overall normalized enrichment score (with FWER=familywise error rate) for each gene set E) Pathway enrichment results for several gene classes: genes strongly up/down regulated in *IGF2BP1* KO cells and genes strongly enriched or depleted in the IGF2BP1 RIP-Seq dataset. For each pathway, shown are the hypergeometric adjusted p-values for each gene class. F) Rank distribution plots of genes in selected functional categories. For each pathway, the x axis represents the gene's rank based on RNA-Seq PC1 loadings, which segregates between genes more expressed in IGF2BP1 KO cells (right) and wild type cells (left). The y axis represents the gene's rank based on RIP-Seq PC1 loadings, which positions RIP-enriched genes on top, and depleted genes at the bottom. Shown are selected gene names of top-ranked genes in each pathway. G) GSEA results of leukemia-associated genes in *IGF2BP1* KO Reh cells. X axis represents the pre-ranked list of genes based on PC1 loadings, which segregates between genes more expressed in *IGF2BP1* KO cells (left) and wild type cells (right). Segment plots (bottom) highlight the position of genes from several genesets identified as up/down regulated in two independent studies comparing *ETV6-RUNX1* with *MLL* and *E2A-PBX1* rearranged leukemias. The vertical axis in line plots (top) represents the cumulative Enrichment Score (ES) from GSEA, and NES is the overall normalized enrichment score (with FWER=familywise error rate) for each gene set. Color-coded names for some genes in selected gene sets are shown

Figure 4

Functional validation of NFκB and PI3K pathways A) Schematic of the NFκB-luciferase reporter assay B) NFκB induction by TNFα (25ng/mL) determined by measuring luciferase activity after BTYNB mediated inhibition of IGF2BP1 in Reh-NFκB-Luc-dTomato cells. Real Time PCR-based validation of IGF2BP1 targets identified from the RIP-Seq data belonging to the C) NFκB and D) PI3K-Akt pathways in the Indian patient cohort (Total n = 111; E6R1+ n= 39, E6R1- (Other translocations) n= 26, No translocation n= 46) and MACS sorted CD19+ B-cell population as controls (n=5) (t test; p * <0.05, ** <0.01, *** <0.005, **** <0.0001)

Figure 5

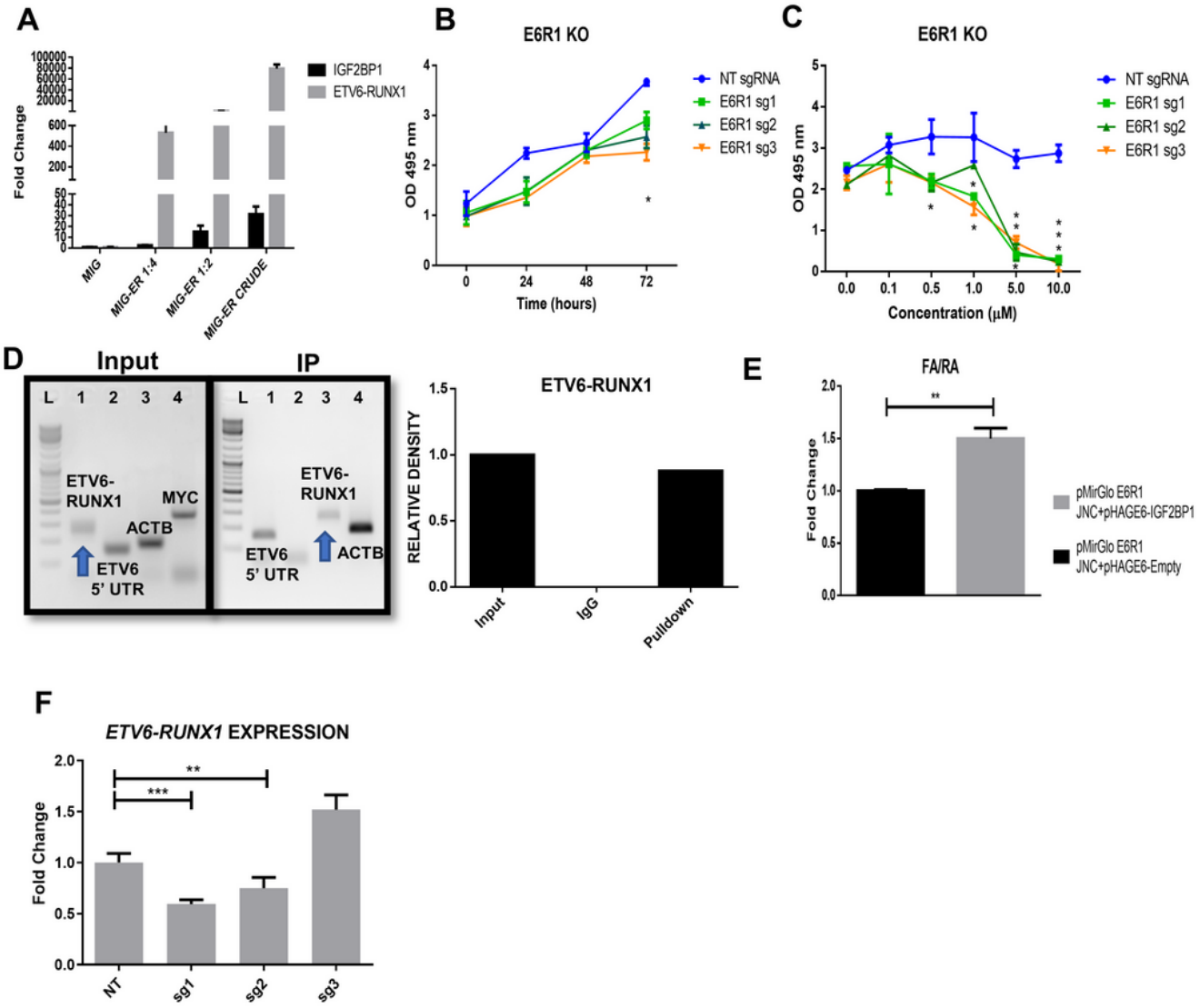

Figure 5

Feedback regulation between ETV6-RUNX1 and IGF2BP1 A) Real Time PCR shows dose dependent increase in *IGF2BP1* levels after overexpression of *ETV6-RUNX1* fusion transcript in 7OZ/3 B) Cell proliferation assay (MTS) shows reduced proliferation of *ETV6-RUNX1* KO Reh-Cas9 cells C) Reversal of prednisolone resistance after *ETV6-RUNX1* KO in Reh-Cas9 cells determined after 72 hours using MTS assay (t-test; p * <0.05, ** <0.01, *** <0.005, **** <0.0001) D) RT-PCR of both Input and

Immunoprecipitated RNA fraction for different known targets of IGF2BP1: ETV6-RUNX1 junction (298 bp), MYC CRD region (357 bp) and 5’ UTR of ETV6 (154 bp) followed by agarose gel electrophoresis. This reveals ETV6-RUNX1 and 5’-ETV6 as targets; β-actin 3’ UTR (184 bp) was used as a positive control E) Dual luciferase assay in 293T cells reveals stabilization of the ETV6-RUNX1 junction by IGF2BP1 F) Effect of *IGF2BP1* KO on *ETV6-RUNX1* fusion transcript stability as determined by qRT-PCR.

Figure 6

IGF2BP1 and ETV6-RUNX1 promote progenitor expansion in the mouse bone marrow A) Bone marrow cell counts showing significantly high numbers in the combination group expressing ETV6-RUNX1 and IGF2BP1 B) Double positive (GFP+ mCherry+) ratio in the bone marrow and representative FACS plots showing clonal expansion C)-F), Quantitation (percentage and absolute counts) of Lineage negative cells, Hematopoietic stem cells, lymphoid-primed multi-potential progenitors, common lymphoid progenitors in the bone marrow of the mice belonging to different groups at 16 weeks after bone marrow transplant with representative FACS plots (n= 8 in each group; t-test; p * <0.05, ** <0.01, *** <0.005, **** <0.0001).

Figure 7

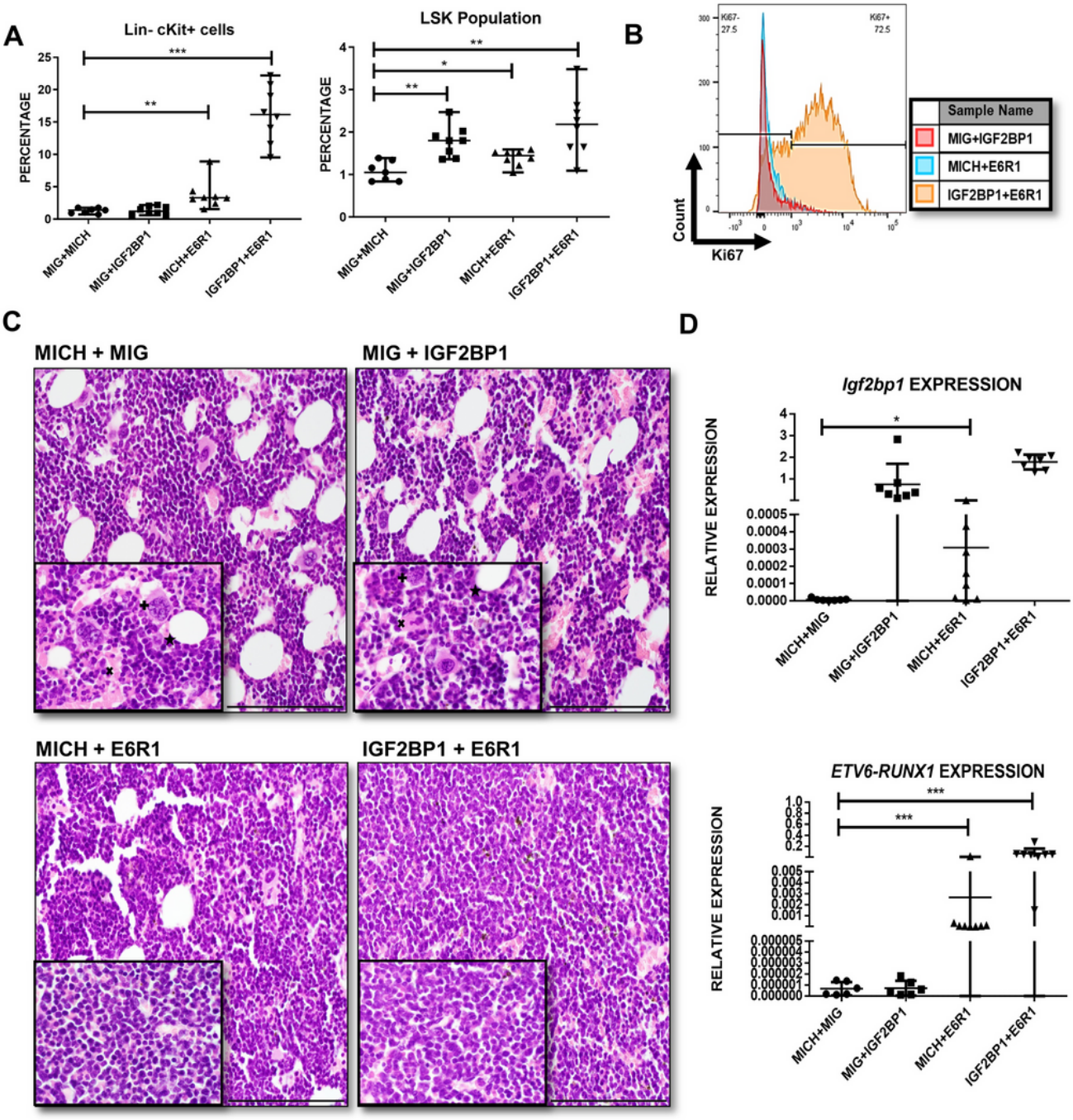

Figure 7

Histopathological analysis of bone marrow architecture after IGF2BP1 and ETV6-RUNX1 overexpression

A) Quantitation of Lin- c-Kit+ cells and Lin- c-Kit+ Sca1+ cells (LSK population) in different mouse groups B) Ki67 positivity in the lineage negative cells of the bone marrow belonging to different groups C) Histologic imaging of bone marrow of mice belonging to different groups; *fat globules,

+megakaryocytes, X: vascular space; Scale bar:100 microns (200X) D) Quantitation of *Igf2bp1* and ETV6-RUNX1 expression in mouse bone marrow (t-test; p * <0.05, ** <0.01, *** <0.005, **** <0.0001)

Supplementary Files

This is a list of supplementary files associated with this preprint. Click to download.

- SupplementaryData.xlsx
- SupplementaryMethodsTables.docx